Mass yield distributions and fission modes in photofission of ^{238}U below 20 MeV

B. S. Ishkhanov, A. A. Kuznetsov, and K. A. Stopani
Lomonosov Moscow State University, Department of Physics,
Skobeltsyn Institute of Nuclear Physics, Moscow, 119991 Russia
(Dated: December 10, 2014)

Photon activation technique is used to obtain photofission mass distributions of ^{238}U in a bremsstrahlung beam with end-point energies 19.5, 29.1, 48.3, and 67.7 MeV. The weights of the symmetric (SL) and asymmetric (STI and STII) modes in the mass distributions of photofission of ^{238}U at the average excitation energies of up to 20 MeV are calculated on the basis of the obtained results and other available data. The weight of the SL mode increases by about 10 times as the average excitation energy increases from 9 to 20 MeV, while the weight of the STI mode decreases by 2 times, and the weight of the STII mode slightly increases. It is shown that the peak-to-valley ratios in photofission of ^{238}U and neutron-induced fission of ^{235}U are very close across almost the whole studied energy range. A similar conclusion is made concerning the behavior of asymmetric and symmetric fission modes in photofission of ^{238}U and neutron-induced fission of ^{235}U.

I. INTRODUCTION

Fission is one of the most studied nuclear processes. However, there are still areas where new and reliable data are needed both for fundamental nuclear science and applied developments. One of these areas is the problem of accurate model description of fragment mass distributions in photon-induced fission, or photofission. Among the examples of its practical importance one can name subcritical nuclear reactor designs (accelerator driven systems), that rely on the spallation reaction triggered by high energy protons [1, 2], and a gamma-ray emission, which often follows this reaction, can trigger photofission and affect functioning of the reactor. Another possible practical application is the transmutation and re-processing of nuclear waste in photonuclear reactions using high-intensity photon beams where the photofission process also plays an important role [3, 4]. Availability of reliable data on cross sections and mass distributions of photofission is also desirable for development of highly intense impulse sources of fast neutrons based on electron accelerators [5, 6].

Since full experimental data are not available in the whole range of nuclear masses and photon energies, model simulations are often used in practical applications [7, 8]. For the purpose of refinement of numeric calculations the most important experimental input for the models comes from the parameters of the fission barrier at different excitation energies. The primary source of this information are distributions of fission fragments, which directly reflect the stage of formation of the fragment masses, as well as the behavior of the potential energy surface under symmetric and asymmetric nuclear deformations which ultimately result in fission.

Theoretical calculations of the potential energy surface in the multi-dimensional deformation space during fission show that the transition from the initial excited state to the point of scission into two fragments can be accomplished along several different trajectories, corresponding to distinct valleys on the potential energy surface [9, 10]. Each of these trajectories forms a fission barrier, which is double-humped in the case of actinide nuclei. Within the multimodal fission model (MM-RNRM [9]) the potential energy valleys correspond to fission modes and the resulting mass distribution is understood as a sum of contributions from three different fission modes: the symmetric SL mode and the asymmetric modes STI and STII. The contribution of each mode is determined by the probability of tunneling through the potential barrier of the particular mode, and, hence, on the shape and height of the barrier, the number of transition states, and their energies above the barrier. Predictions of the multimodal model agree with the experimental mass distributions of neutron- and proton-induced fission. The main factor determining the shape of the fission barrier of asymmetric modes in the model [9] is the nuclear shell structure, in the form of the shell corrections [11]. The amount of shell effects depends on the nuclear temperature during fission [12], and the temperature dependence is introduced by means of the so-called shell effects damping function. Exponential damping of the shell effects, which is considered in [13], leads to gradual vanishing of the asymmetric modes at higher excitation energies and the rate of damping is determined by the damping energy parameter $E_0 \approx 15$ MeV. Based on the analysis of charge distributions of fission fragments a different value is suggested in [14], $E_0 \approx 60$ MeV.

The shape and the width of the valley on the potential energy surface between the second saddle point and the point of scission into fragments affect the stiffness (and, thus, the width of the distribution) of the corresponding fission mode, and, therefore, can be analyzed using the fragment distributions. In neutron-induced fission the properties of fission modes were studied for the actinide nuclei in [15]. Systematic relationships for yields of fission products in neutron- and proton-induced fission of heavy nuclei and a parameterization of fission product yields as a function of the fissioning nucleus and the excitation energy were obtained in [16].

A consistent description of the dependence of the fission modes on the excitation energy in photofission has not yet been published. There are only few works where contributions of different components of the mass distributions were estimated. Contributions of fission modes in the mass distribution were calculated in [17] at

two energies of the electron accelerator (50 MeV and 3.5 GeV). The presence of different fission modes is pointed at in [18], though no quantitative estimates are given. Contributions of the fission modes were estimated in [19] using bremsstrahlung photons with end-point energies from 6 to 10 MeV.

In the present work the photon activation technique is used to measure photofission mass distributions of ^{238}U using bremsstrahlung with end-point energy 19.5, 29.1, 48.3, 67.7 MeV. Using the obtained results and available data from other works [17, 18, 20–22] the relative contributions of fission modes in the excitation energy range from 5 to 20 MeV are obtained. The behavior of photofission modes of ^{238}U is compared to the behavior of the modes of the neutron-induced fission of ^{235}U and the results of the systematics [16] for neutron-induced fission of the ^{238}U compound nucleus.

II. EXPERIMENTAL TECHNIQUE

A. Experimental setup

The photon activation technique was used to measure photofission fragment yields from ^{238}U. The experimental setup and the data analysis procedures are described in [23–26]. The experiment was performed using bremsstrahlung radiation produced by the 70 MeV race-track microtron of the Skobeltsyn Institute of Nuclear Physics of the Moscow State University [27] at the electron energies T = 19.5, 29.1, 48.3, and 67.7 MeV. A 0.2-mm-thick aluminum disk (100 mm in diameter), onto which a 1-mg cm^{-2}-thick film of natural uranium was deposited, was used as a target. The target was irradiated by bremsstrahlung radiation produced by the electron beam. A 2.2-mm-thick tungsten target was used as a bremsstrahlung converter. Each irradiation took 3 ÷ 7.5 hr at average beam current of about 10 nA. After each irradiation series of gamma-ray spectra of induced activity were measured using an HPGe detector with relative efficiency 30% and energy resolution of 0.9 keV at 122 keV, 1.9 keV at 1.33 MeV. Each series of spectrum acquisitions was started within 2 min after the corresponding irradiation and lasted for several days to several weeks. After acquisition the spectra were analyzed and yields of different isotopes were calculated from the time dependence of the peak areas.

B. Data analysis

The nuclei produced as a result of fission are interconnected by chains of decays. Each unstable nucleus can be produced both in fission and as a result of β^--decays of other members of the chain. The activation technique allows to measure the yields of isotopes with half lives of several minutes and greater. Thus, only fragment yields after prompt neutron emission are obtained. For majority of the isotopes the employed technique allows to determine only the cumulative yield, which includes its production both in fission and in decays of the whole chain of the parent isobar nuclei.

The cumulative yield of a fission fragment $Y_{\rm cum}$ was calculated using the following expression:

$$Y_{\rm cum} = \frac{N_0 \lambda}{(1 - e^{-\lambda t_{\rm rad}})}, \tag{1}$$

where λ is the decay constant, $t_{\rm rad}$ is the duration of the irradiation, and N_0 is the number of the nuclei in the target at the end of the irradiation. N_0 was determined from the areas of corresponding photopeaks in the measured gamma-ray spectra:

$$N_0 = \frac{S}{k} \frac{1}{e^{-\lambda(t_1 - t_{\rm rad})} - e^{-\lambda(t_2 - t_{\rm rad})}}, \tag{2}$$

where S is the area of the peak, summed over the measured spectra, t_1 and t_2 denote the times when the measurement started and ended, k is a coefficient equal to the product of the detector efficiency at the peak's energy, the relative intensity of the spectral line, and the true coincidence correction factor. Generally, for different peaks of the same decaying fragment the yields were obtained in this way independently, and a weighted average was calculated subsequently. Two typical spectra of the uranium target after irradiation at T = 29.1 MeV with corresponding photopeaks of fission fragments are shown in Fig. 1.

When the independent yield could be calculated (i.e., the decays of parent nuclei of the chain were visible in the spectra), the differential equations describing accumulation and decay of the mass chain elements were analytically solved, and the resulting solutions were used to fit the experimental decay curves. As an example we show the expressions, that were used to obtain independent yields for chain with 3 elements, described by a decay scheme "isotope 1 → isotope 2 → isotope 3":

$$Y_2 = \frac{\lambda_2 N_{20}}{1 - e^{-\lambda_2 t_{\rm rad}}} - Y_1 \frac{\lambda_2 (1 - e^{-\lambda_1 t_{\rm rad}}) - \lambda_1 (1 - e^{-\lambda_2 t_{\rm rad}})}{(\lambda_2 - \lambda_1)(1 - e^{-\lambda_2 t_{\rm rad}})}, \tag{3}$$

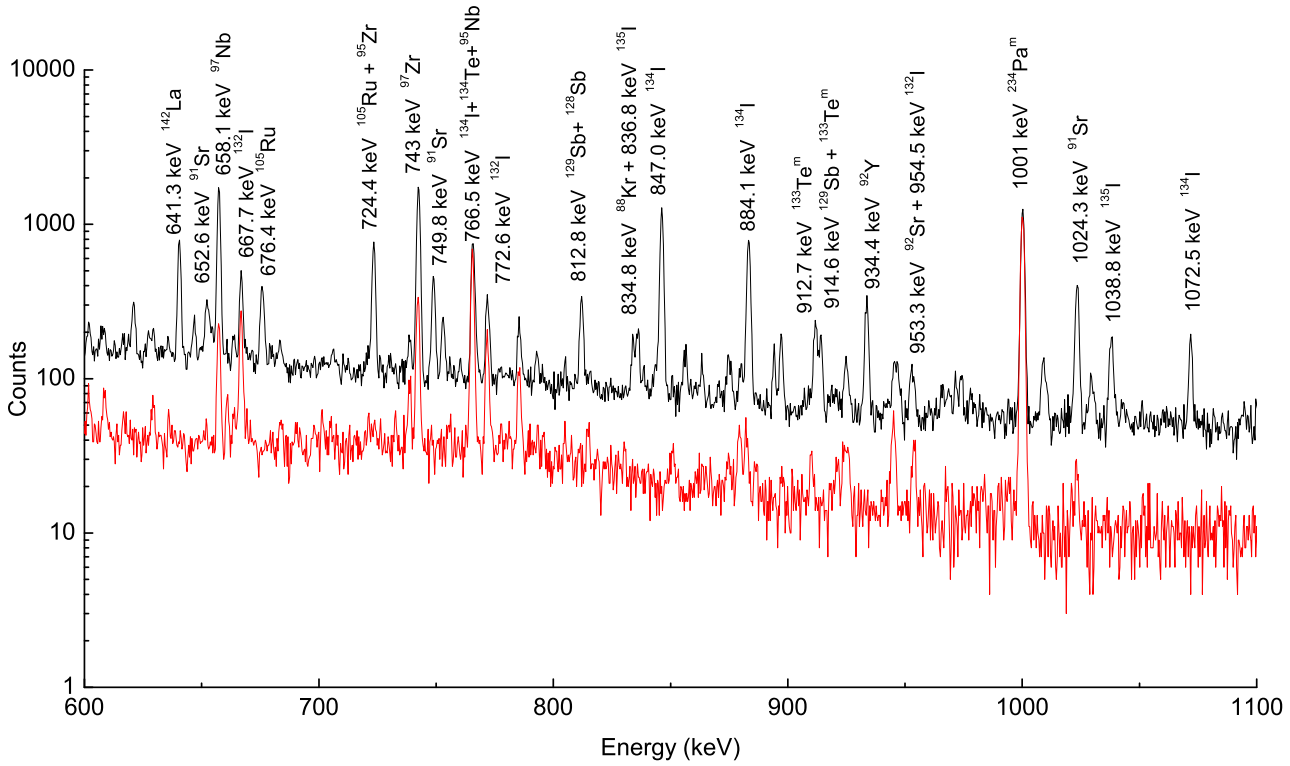

Figure 1. (Color online) Gamma-ray spectra of induced activity of uranium target after irradiation at $T = 29.1$ MeV, summed over 10 hours. From top to bottom: (1) measurement 1 hr after irradiation; (2) measurement 3 days after irradiation.

where Y_2 is the independent yield of the second isotope of the chain, Y_1 is the cumulative yield of the first isotope, obtained using Eq. (1), λ_1 and λ_2 are the corresponding decay constants, and N_{20} is the number of nuclei of the second isotope at the end of the irradiation, which is determined as follows:

$$N_{20} = \frac{S}{k_2(e^{-\lambda_2(t_1-t_{\rm rad})} - e^{-\lambda_2(t_2-t_{\rm rad})})} + \frac{N_{10}\lambda_1}{\lambda_2-\lambda_1} - \frac{N_{10}\lambda_2}{\lambda_2-\lambda_1}\cdot\frac{(e^{-\lambda_1(t_1-t_{\rm rad})} - e^{-\lambda_1(t_2-t_{\rm rad})})}{(e^{-\lambda_2(t_1-t_{\rm rad})} - e^{-\lambda_2(t_2-t_{\rm rad})})}, \quad (4)$$

where N_{10} is the number of nuclei of the first isotope, which is obtained similarly to Eq. (2), and k_2 is calculated for the second isotope analogously to k.

By definition the mass yield $Y_{\rm MY}(A)$ is a sum of independent yields of all isotopes of the isobaric chain with the given mass number A, or the cumulative yield of the long-lived isotope at the end of the chain.

Direct determination of the summed yield of fission fragments with a given mass number A from the sum of yields of all elements of the mass chain was not possible (due to a very long- or short-lived decay, or due to absence of detectable gamma lines), and the following procedure was used to estimate the mass yield from the charge number distribution. The charge number distribution of photofission products with a given mass number A can be approximated using the Gaussian function [28]:

$$Y_{\rm IY}(A,Z) = \frac{Y_{\rm MY}(A)}{\sqrt{\pi C}}\ e^{-\frac{(Z-Z_P)^2}{C}}, \quad (5)$$

where $Y_{\rm IY}(A,Z)$is the independent yield of the photofission product with the given A and Z, $Y_{\rm MY}(A)$ is the mass yield of the isotopes with the mass number A, Z_p is the most probable charge number of the nuclei from the given mass chain, C is the width of the charge number distribution. The $Y_{\rm MY}(A)$ value was determined from available independent and cumulative yields by normalizing the observed points to expression (5).

The most probable charge number Z_p was calculated for each chain of isobar nuclei using the expressions [29]:

$$Z_p = Z_{\rm UCD} \pm \Delta Z_p, \quad Z_{\rm UCD} = (Z_F/A_F)(A+\nu_{L,H}), \quad (6)$$

where $Z_F = 92$ and $A_F = 238$ are the charge and mass numbers of the initial nucleus, $Z_{\rm UCD}$ is the most probable charge number, determined from the assumption that the ratio of neutrons to protons in fission fragments is the same as in the initial nucleus [30], and the charge polarization ΔZ_p was calculated from the systematics [16]. The "+" and "−" signs denote, respectively, the heavy and the light fragments. ν_L and ν_H are the numbers of prompt neutrons emitted from the light and heavy fragments, estimated as described in [31]. As shown in

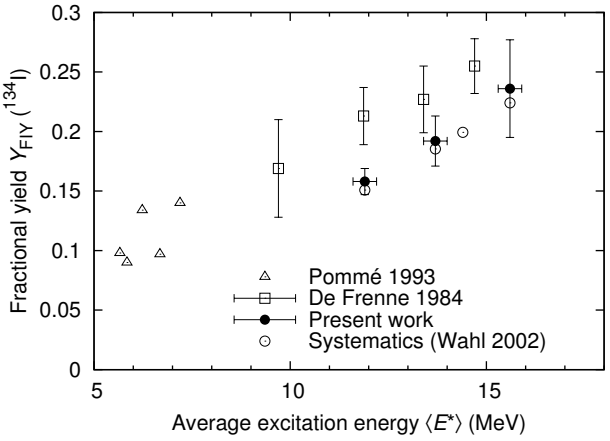

Figure 2. Relative independent yield of the $^{134}_{53}$I isotope as a function of the average excitation energy of ^{238}U: (dots) present work; Pommé 1993: [33]; De Frenne 1984: [34]; empty dots (Wahl 2002) represent relative independent yield of the $^{134}_{53}$I isotope calculated from the systematics [16] for neutron- and proton-induced fission.

works [21, 32, 33], for excitation energies less than 30 MeV the width of the charge number distribution shows only a slight dependence on its value. For photofission of ^{238}U the width of the charge number distribution $C \approx 0.8$ [32].

An example of determination of fission fragment yields is shown in Fig. 2. Our technique allows to determine the cumulative yield of the $^{134}_{52}$Te isotope and the independent yield of the $^{134}_{53}$I isotope. Figure 2 shows the relative independent yield of the $^{134}_{53}$I isotope as a function of the average excitation energy of the nucleus. By definition, the fraction independent yield $Y_{\rm FIY}(A,Z)$ is equal to the isotope's independent yield $Y_{\rm IY}(A,Z)$ normalized by the total yield $Y_{\rm MY}(A)$ of the decay chain with the given mass number: $Y_{\rm FIY}(A,Z) = Y_{\rm IY}(A,Z)/Y_{\rm MY}(A)$. At low excitation energies the most probable charge number of the mass chain with $A = 134$ corresponds to the even magic $^{134}_{52}$Te. As the excitation energy of ^{238}U increases from 6 to 16 MeV the relative independent yield of the odd iodine isotope $^{134}_{53}$I increases by 2.5 times, from 10% to 25% of the total mass yield. The obtained results are in agreement with the predictions of the systematics [16], which is based on the experimental data on neutron- and proton-induced fission.

As a final step to obtain the mass yields one has to take into account the effect of delayed neutron emission. Our technique allows to start measurements of the radioactivity of the fission products in about several minutes after the irradiation. By this moment almost all delayed neutrons are already emitted, which results in a shift of the cumulative yields. The number of emitted delayed neutrons depends on the particular mass chain. The relative number of delayed neutrons can be estimated by folding the charge number distribution with the probability of delayed neutron emission from a particular nucleus. The delayed neutron correction increases the observed mass yield $Y_{\rm MY}(A)$ due to emission of delayed neutrons from the neighboring mass chain $A+1$, while emission of delayed neutrons by the A chain itself results in a decrease of the observed mass yield.

$$\Delta Y_{\rm MY}(A) = \sum_i Y_{{\rm IY}\,i}(A+1, Z_i) \cdot W_d(A+1, Z_i) - \sum_i Y_{{\rm IY}\,i}(A, Z_i) \cdot W_d(A, Z_i), \tag{7}$$

where $W_d(A, Z_i)$ is the probability of a delayed neutron emission by a given isotope (A, Z_i), $Y_{{\rm IY}\,i}(A, Z_i)$ is the independent yield of the (A, Z_i) isotope.

As a result of the analysis the mass distributions of fragments of photofission of ^{238}U were obtained at four values of the bremsstrahlung end-point energy $T = 19.5, 29.1, 48.3, 67.7$ MeV. The obtained mass yields are normalized to the yield of the photoneutron reaction ^{238}U(γ, n)^{237}U.

To compare the obtained fission product yields with results of other experiments the average excitation energies of the initial nucleus were calculated. The average excitation energy $\langle E^* \rangle$ of the fissioning nucleus was calculated using the following expression:

$$\langle E^*(T) \rangle = \frac{\int\limits_0^T N(T,E)\sigma_{\gamma,F}(E)E dE}{\int\limits_0^T N(T,E)\sigma_{\gamma,F}(E) dE}, \tag{8}$$

where $N(T,E)$ is the bremsstrahlung photon spectrum, T is the electron accelerator energy (i.e., the end-point energy of the bremsstrahlung spectrum), $\sigma_{\gamma,F}(E)$ is the photofission cross section at the photon energy E. The bremsstrahlung spectrum for each accelerator energy was calculated using the GEANT4 [35] package. The

Table I. Experimental mass yields in photofission of ^{238}U. Relative mass yields are normalized to the yield of the ^{238}U(γ,n)^{237}U reaction at the corresponding energy. Fraction mass yields Y_{FMY} are given per 100 fission reactions, i.e. $\sum_A Y_{\mathrm{FMY}} = 200$.

	Relative mass yield $Y_{\mathrm{MY}}/Y(\gamma,\mathrm{n}) \times 10^3$				Fraction mass yield Y_{FMY}			
A	19.5 MeV	29.1 MeV	48.3 MeV	67.7 MeV	19.5 MeV	29.1 MeV	48.3 MeV	67.7 MeV
84	1.90 ± 0.45	2.94 ± 0.71	1.62 ± 0.49	5.01 ± 1.41	0.62 ± 0.15	0.79 ± 0.19	0.44 ± 0.13	1.14 ± 0.32
85	3.69 ± 0.25	4.18 ± 0.24	3.72 ± 0.10	5.81 ± 0.24	1.21 ± 0.08	1.13 ± 0.07	1.01 ± 0.03	1.33 ± 0.06
87	5.17 ± 0.32	5.86 ± 0.35	4.81 ± 0.32	7.27 ± 0.57	1.70 ± 0.10	1.58 ± 0.10	1.31 ± 0.09	1.66 ± 0.13
88	6.08 ± 0.67	7.69 ± 0.52	7.12 ± 0.79	9.13 ± 0.83	1.99 ± 0.22	2.07 ± 0.14	1.94 ± 0.22	2.08 ± 0.19
89	10.80 ± 1.50	9.25 ± 1.01	9.15 ± 1.26	14.25 ± 2.14	3.54 ± 0.49	2.49 ± 0.27	2.49 ± 0.34	3.25 ± 0.49
91	14.31 ± 1.59	16.17 ± 0.83	16.49 ± 0.30	17.44 ± 1.28	4.69 ± 0.52	4.36 ± 0.22	4.49 ± 0.08	3.98 ± 0.29
92	15.77 ± 1.03	19.06 ± 1.05	17.19 ± 0.62	21.32 ± 0.89	5.17 ± 0.34	5.14 ± 0.28	4.68 ± 0.17	4.86 ± 0.20
93	15.71 ± 2.50	19.55 ± 3.03	18.64 ± 1.06	23.30 ± 2.02	5.15 ± 0.82	5.27 ± 0.82	5.08 ± 0.29	5.31 ± 0.46
94	16.34 ± 1.55	20.24 ± 1.72		25.03 ± 3.03	5.36 ± 0.51	5.45 ± 0.46		5.71 ± 0.69
97	17.19 ± 0.40	21.07 ± 0.58	21.58 ± 2.04	25.11 ± 0.53	5.64 ± 0.13	5.68 ± 0.16	5.88 ± 0.55	5.73 ± 0.12
99	17.76 ± 0.14	22.31 ± 0.31	21.62 ± 0.12	24.31 ± 0.28	5.83 ± 0.05	6.01 ± 0.08	5.89 ± 0.03	5.54 ± 0.06
101	17.75 ± 2.11	22.01 ± 1.72	21.65 ± 1.48	24.51 ± 2.30	5.82 ± 0.69	5.93 ± 0.46	5.90 ± 0.40	5.59 ± 0.52
104	10.31 ± 0.79	13.24 ± 0.77	11.46 ± 0.81	15.87 ± 1.45	3.38 ± 0.26	3.57 ± 0.21	3.12 ± 0.22	3.62 ± 0.33
105	8.77 ± 0.54	10.75 ± 1.61	9.50 ± 0.51	13.57 ± 0.57	2.88 ± 0.18	2.90 ± 0.43	2.59 ± 0.14	3.09 ± 0.13
107	3.29 ± 0.42	3.73 ± 0.43	3.90 ± 0.52	7.11 ± 1.33	1.08 ± 0.14	1.01 ± 0.12	1.06 ± 0.14	1.62 ± 0.30
112	0.64 ± 0.11	1.61 ± 0.27	1.93 ± 0.31	2.79 ± 0.36	0.21 ± 0.04	0.43 ± 0.07	0.52 ± 0.09	0.64 ± 0.08
113	0.64 ± 0.09	1.61 ± 0.42	1.90 ± 0.45	2.50 ± 0.56	0.21 ± 0.03	0.43 ± 0.11	0.52 ± 0.12	0.57 ± 0.13
115	0.66 ± 0.12	1.72 ± 0.26	2.09 ± 0.36	2.54 ± 0.24	0.22 ± 0.04	0.46 ± 0.07	0.57 ± 0.10	0.58 ± 0.06
117	0.62 ± 0.13	1.77 ± 0.33	1.94 ± 0.28	2.70 ± 0.35	0.20 ± 0.04	0.48 ± 0.09	0.53 ± 0.08	0.62 ± 0.08
123	0.72 ± 0.09	1.79 ± 0.19	2.10 ± 0.17	2.99 ± 0.36	0.34 ± 0.03	0.48 ± 0.05	0.57 ± 0.05	0.68 ± 0.08
127	1.99 ± 0.27	3.93 ± 1.03	3.92 ± 0.32	4.04 ± 0.44	0.65 ± 0.09	1.06 ± 0.28	1.07 ± 0.09	0.92 ± 0.10
128	2.75 ± 0.36	4.30 ± 0.35	4.05 ± 0.44	4.60 ± 0.53	0.90 ± 0.12	1.16 ± 0.10	1.10 ± 0.12	1.05 ± 0.12
129	4.07 ± 0.53	5.63 ± 0.73	5.22 ± 0.63	6.34 ± 1.08	1.34 ± 0.17	1.52 ± 0.20	1.42 ± 0.17	1.45 ± 0.25
130		8.12 ± 1.36				2.19 ± 0.37		
131	11.67 ± 1.47	11.79 ± 2.12	14.01 ± 1.26	16.31 ± 1.22	3.83 ± 0.48	3.18 ± 0.57	3.82 ± 0.34	3.72 ± 0.28
132	15.35 ± 0.15	16.94 ± 0.23	18.66 ± 0.14	21.36 ± 0.28	5.04 ± 0.05	4.56 ± 0.06	5.08 ± 0.04	4.87 ± 0.06
133	20.15 ± 0.46	23.36 ± 0.55	23.13 ± 0.64	25.52 ± 1.09	6.61 ± 0.15	6.29 ± 0.15	6.30 ± 0.17	5.82 ± 0.25
134	20.89 ± 0.86	24.65 ± 0.97	23.90 ± 0.44	27.62 ± 2.06	6.85 ± 0.28	6.64 ± 0.26	6.51 ± 0.12	6.30 ± 0.47
135	19.31 ± 0.46	23.50 ± 0.68	21.36 ± 0.39	26.61 ± 1.78	6.33 ± 0.15	6.33 ± 0.18	5.82 ± 0.11	6.07 ± 0.41
138	17.58 ± 1.39	22.17 ± 1.17	21.35 ± 1.60		5.77 ± 0.46	5.97 ± 0.32	5.82 ± 0.44	
139	18.27 ± 0.42	22.04 ± 0.48	19.75 ± 0.82	24.95 ± 0.81	5.99 ± 0.14	5.94 ± 0.13	5.38 ± 0.22	5.69 ± 0.18
140	17.42 ± 1.24	19.51 ± 2.03	19.93 ± 0.81	23.22 ± 2.50	5.71 ± 0.41	5.26 ± 0.55	5.43 ± 0.22	5.29 ± 0.57
141	14.91 ± 2.09	19.37 ± 2.71		22.97 ± 1.66	4.89 ± 0.68	5.22 ± 0.73		5.24 ± 0.38
142	14.85 ± 1.78	18.08 ± 1.17	15.97 ± 0.50	19.70 ± 2.42	4.87 ± 0.58	4.87 ± 0.32	4.35 ± 0.14	4.49 ± 0.55
143	13.75 ± 0.25	15.64 ± 0.34	12.26 ± 0.24	18.33 ± 0.49	4.51 ± 0.08	4.21 ± 0.09	3.34 ± 0.06	4.18 ± 0.11
146	9.97 ± 1.14	11.02 ± 0.85	9.15 ± 0.88	14.37 ± 1.58	3.27 ± 0.37	2.97 ± 0.23	2.49 ± 0.24	3.28 ± 0.36
149	3.79 ± 0.33	5.23 ± 0.74	4.00 ± 0.51	5.45 ± 1.01	1.24 ± 0.11	1.41 ± 0.20	1.09 ± 0.14	1.24 ± 0.23
151	2.21 ± 0.37	2.08 ± 0.37	2.17 ± 0.39	2.02 ± 0.44	0.73 ± 0.12	0.56 ± 0.10	0.59 ± 0.11	0.46 ± 0.10

photoneutron and photofission reaction cross sections were measured in several experimental works [36–38]. We used the evaluated photofission cross section from Ref. [39], which was obtained from the experimental cross sections and which takes into account shortcomings of the neutron multiplicity sorting technique employed in experimental measurements. It has been shown in [40] that under 20 MeV the fissility of ^{238}U obtained experimentally is in agreement with the one determined using the evaluation [39]. The procedure of calculation of the average excitation energy is shown schematically in Fig. 3.

The bremsstrahlung energies shown above correspond to the following average excitation energies: $\langle E^* \rangle = 11.9 \pm 0.3, 13.7 \pm 0.3, 14.4 \pm 0.3, 15.6 \pm 0.3$ MeV.

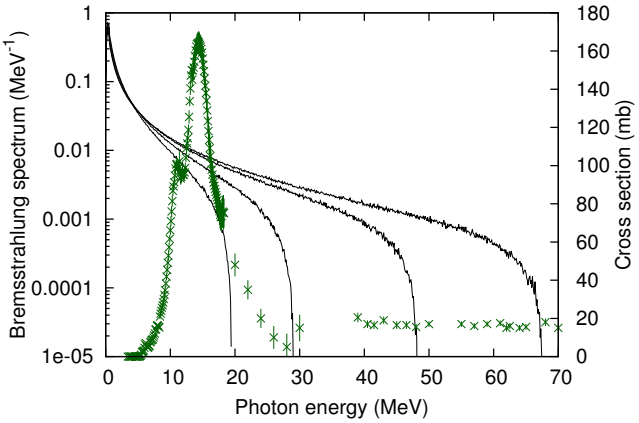

Figure 3. (Color online) Evaluated cross section of the photofission reaction on ^{238}U ([39], right axis) and simulated bremsstrahlung spectra at $T = 19.5$, 29.1, 48.3, 67.7 MeV (left axis) used to calculate the average excitation energies of photofission.

III. DISCUSSION OF THE RESULTS

The fraction mass yield distributions $Y_{\mathrm{FMY}}(A)$ of photofission fragments of ^{238}U per 100 photofission reactions, defined as

$$Y_{\mathrm{FMY}}(A) = 200 \times \frac{Y_{\mathrm{MY}}(A)}{\sum Y_{\mathrm{MY}}}, \tag{9}$$

for the end-point energies of bremsstrahlung $T = 19.5, 29.1, 48.3, 67.7$ MeV are shown in table I.

Figure 4 shows the same data in graphical form as a function of the average excitation energy of ^{238}U. A comparison of the obtained distributions with available photofission data from other works with end-point energies of bremsstrahlung from 15 to 30 MeV is shown in Fig. 5. The final mass distributions can be viewed as a result of competition of collective modes, which lead to either symmetric or asymmetric formation of fission fragments [41, 42]. The latter is a manifestation of nuclear shell effects, which experience damping as the nuclear excitation energy increases. This behavior can be seen in Fig. 6, which shows the energy dependence of the peak-to-valley ratio, i.e. the ratio between the maximum and the minimum of the mass distribution. Figure 6 shows the peak-to-valley ratio p/v as a function of the average excitation energy obtained in [17, 42–46] for photofission of ^{238}U, and in [47, 48] and [49–54] for fission of, respectively, ^{235}U and ^{238}U, induced by monoenergetic neutrons. Our results agree with the general tendency of increasing contribution of the symmetric fission mode as the excitation energy increases.

The value of the peak-to-valley ratio decreases exponentially when the excitation energy increases in the range from 6 to 16 MeV, but at higher energies the ratio is almost constant. This behavior can be explained by the fact that at lower excitation energies only fission (γ, fiss) and neutron emission (γ, n) are possible, and as energy increases the reaction channel of neutron emission and subsequent fission (γ, n fiss) becomes possible. In [36] it has been shown that the energy threshold of the latter reaction in ^{238}U is about 12 MeV. After emission of a neutron the resulting ^{237}U nucleus undergoes fission at a lower excitation energy:

$$E^{*\prime}(^{237}\mathrm{U}) = E^{*}(^{238}\mathrm{U}) - B_n(^{238}\mathrm{U}) - T_n \tag{10}$$

(where B_n is the neutron separation energy of ^{238}U, T_n is the kinetic energy of the outgoing neutron), effectively contributing a larger value of the peak-to-valley ratio.

The behavior of the peak-to-valley ratio is very close for photofission of ^{238}U and neutron-induced fission of ^{235,238}U. The only region where the ratio of asymmetric and symmetric fission is different is from 12 to 15 MeV for ^{235}U, while at other energies the values are the same within the error limits. This can probably be attributed to different fissilities and neutron separation energies of the compound nuclei. The energy threshold of fission with a preceding neutron emission (γ, n fiss) is lower for the ^{239}U compound nucleus, and thus the second-chance fission process is more important in neutron-induced fission of ^{238}U. It can be noted that from 12 to 15 MeV the peak-to-valley ratio in neutron-induced fission of ^{235}U decreases somewhat slower than in photon- and neutron-induced fission of ^{238}U.

Further analysis of the mass distributions of photofission of ^{238}U is focused on the structure which can be seen at the peaks of the distribution at lower excitation energies of the compound nucleus (of the order of the fission barrier height). According to [9] the presence of relatively narrow maxima corresponding to the mass numbers $A \approx 134$ and $A \approx 101$ in addition to the main peaks at $A \approx 139$ and $A \approx 96$ is a manifestation of

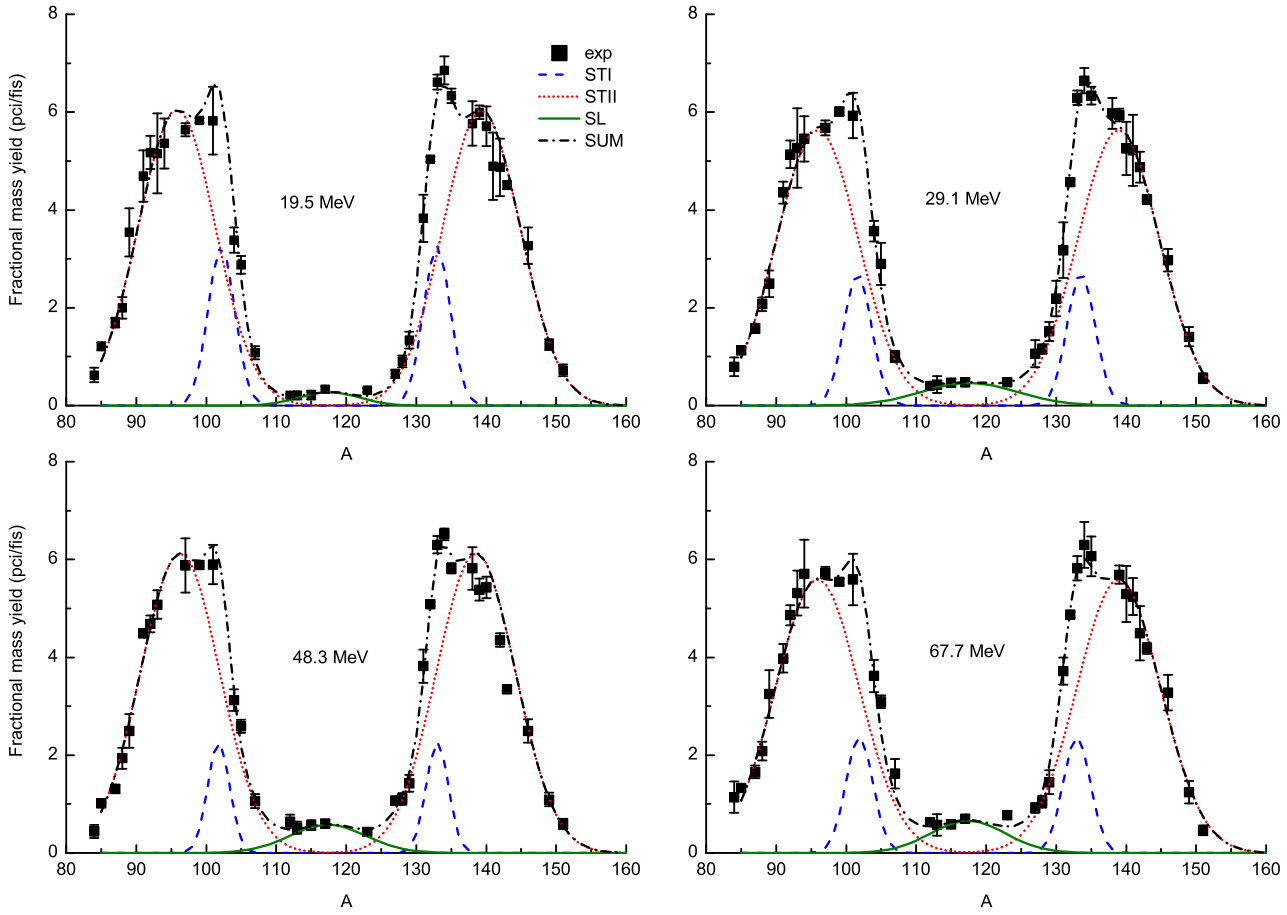

Figure 4. (Color online) Fraction mass yields (Y_{FMY}) of photofission of ^{238}U and results of fitting the distributions with five Gaussian curves at bremsstrahlung end-point energies 19.5, 29.1, 48.3, and 67.7 MeV: experimental data (squares), asymmetric component STI (dashed curve), asymmetric component STII (dotted curve), symmetric component SL (solid curve), sum of the components (dashed-dotted curve).

the asymmetric mode STI which leads to formation of a spherical fragment with $N \approx 82$ and a corresponding light fragment. The pre-neutron mass distributions measured in [18, 19, 55] also show analogous fine structure around the $A = 134$ mass number. It is seen from Fig. 4 that this effect experiences damping as the excitation energy of the initial nucleus increases and it practically disappears when the excitation energy is greater than approximately 15 MeV. This behavior of the asymmetric mode STI as a function of the excitation energy was theoretically described in [9, 12]. Another nuclear effect, which may result in different yields of fragments with neighboring masses at the peaks of the mass distribution, is the even-odd effect, which also experiences damping with the increase of the nucleus' excitation energy [33], but we see no direct signs of its contribution in other regions of Fig. 4.

The obtained mass distributions were decomposed into the components of the multimodal model of fission [9, 10]: the asymmetric STI mode, corresponding to the $N = 82$ magic number, the asymmetric STII mode, corresponding to the deformed shell $N = 86 \div 88$, and the symmetric SL mode. For each mode the distribution of fragment masses is described as a Gaussian function. The total yield of fragments with a given mass number A is described with the following relationship:

$$Y(A) = Y_{\mathrm{SL}}(A) + Y_{\mathrm{STI}}(A) + Y_{\mathrm{STII}}(A) = K_{\mathrm{SL}} \exp\left[-\frac{(A - A_{\mathrm{SL}})^2}{2{\sigma_{\mathrm{SL}}}^2}\right] +$$
$$+K_{\mathrm{STI}} \exp\left[-\frac{(A - A_{\mathrm{SL}} - D_{\mathrm{STI}})^2}{2{\sigma_{\mathrm{STI}}}^2}\right] + K_{\mathrm{STI}} \exp\left[-\frac{(A - A_{\mathrm{SL}} + D_{\mathrm{STI}})^2}{2{\sigma_{\mathrm{STI}}}^2}\right] +$$
$$+K_{\mathrm{STII}} \exp\left[-\frac{(A - A_{\mathrm{SL}} - D_{\mathrm{STII}})^2}{2{\sigma_{\mathrm{STII}}}^2}\right] + K_{\mathrm{STII}} \exp\left[-\frac{(A - A_{\mathrm{SL}} + D_{\mathrm{STII}})^2}{2{\sigma_{\mathrm{STII}}}^2}\right], \qquad (11)$$

where the Gaussian parameters $K_{\mathrm{SL}}, K_{\mathrm{STI}}, K_{\mathrm{STII}}, \sigma_{\mathrm{SL}}, \sigma_{\mathrm{STI}}, \sigma_{\mathrm{STII}}$ are the amplitudes and widths of the symmetric (SL) and asymmetric (STI, STII) fission modes, A_{SL} is the most probable fragment mass number for the symmetric mode, $A_{\mathrm{SL}} - D_{\mathrm{STI}}$, $A_{\mathrm{SL}} + D_{\mathrm{STI}}$ are the most probable mass numbers of the light and heavy fragments

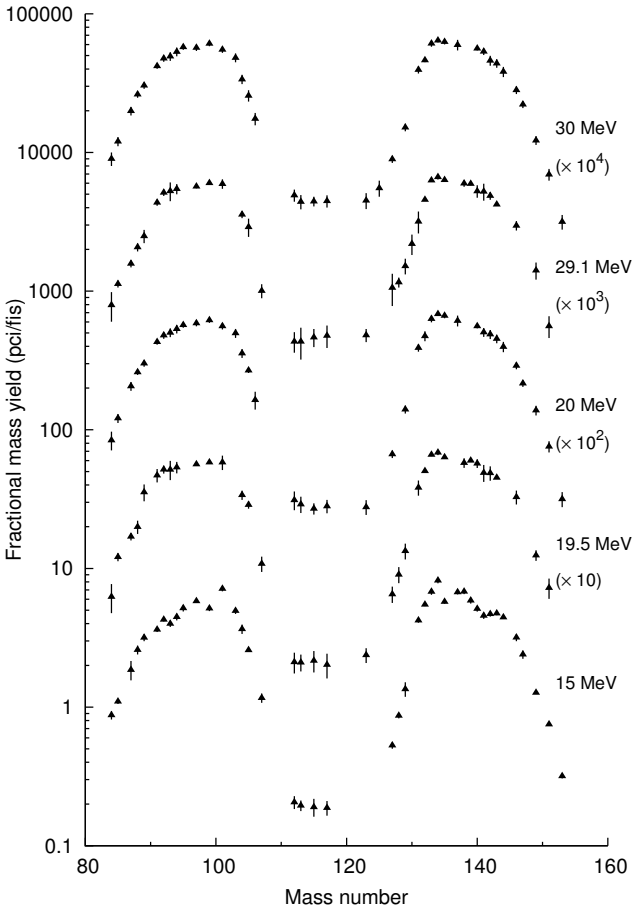

Figure 5. Comparison of the mass yield distributions of photofission at bremsstrahlung end-point energies T from 15 to 30 MeV. From top to bottom: (1) $T = 30$ MeV, $\langle E^* \rangle = 14.7$ MeV (Ref. [21]); (2) $T = 29.1$ MeV, $\langle E^* \rangle = 13.7$ MeV (this work); (3) $T = 20$ MeV, $\langle E^* \rangle = 13.4$ MeV (Ref. [21]); (4) $T = 19.5$ MeV, $\langle E^* \rangle = 11.9$ MeV (this work); (5) $T = 15$ MeV, $\langle E^* \rangle = 11.9$ MeV (Ref. [22]).

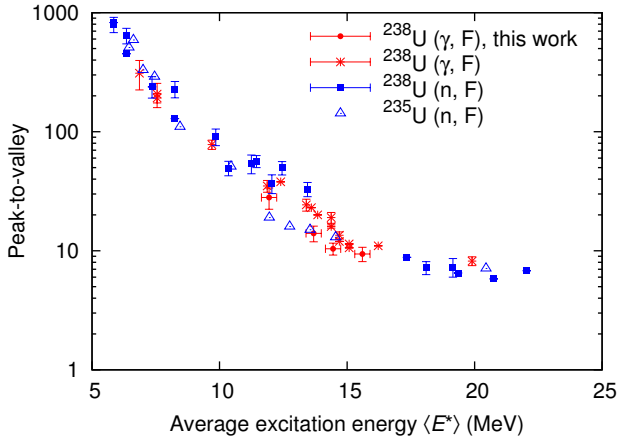

Figure 6. (Color online) Peak-to-valley ratio p/v for photofission of ^{238}U (dots, stars) and neutron-induced fission of ^{235}U (squares) and ^{238}U (triangles) as a function of the average excitation energy $\langle E^* \rangle$. Photofission data from this work (dots) and Refs. [17, 42–46] (stars), neutron-induced fission for ^{238}U from Refs. [49–54], for ^{235}U from Refs. [47, 48].

of the asymmetric mode STI, $A_{\rm SL} - D_{\rm STII}$, $A_{\rm SL} + D_{\rm STII}$ are the most probable mass numbers of the light and heavy fragments of the asymmetric mode STII. Restoration of mode probabilities from the post-neutron distribution can be negatively influenced by the shifting and widening effects in the peaks of the distribution caused by emission of prompt neutrons. To estimate possible errors from these effects we also performed fits with version of Eq. (11) with independent parameters of the light and heavy branches of asymmetric modes. The mode

Table II. Contributions of the fission modes into the mass distributions as a function of the excitation energy of the fissioning nucleus $\langle E^* \rangle$ in photofission of $^{238}_{92}$U.

T, MeV	$\langle E^* \rangle$, MeV	STI	STII	SL	Ref.
6.12	5.66	52.87 ± 6.44	147.13 ± 7.64		[18]
7.33	6.23	48.07 ± 6.29	151.93 ± 7.25		[18]
9.31	7.19	41.57 ± 5.25	158.43 ± 7.21		[18]
11.47	9.09	40.49±7.32	158.73±8.77	0.78±0.98	[22]
12	9.7	47.35 ± 5.19	151.74 ± 5.91	1.22 ± 0.62	[21]
13.39	10.38	47.39 ±10.33	150.58 ±11.92	2.03 ±2.45	[22]
15	11.6	37.67 ±6.43	159.87 ±7.40	2.47 ±1.52	[22]
15	11.9	37.37 ± 4.41	160.37 ± 5.50	2.71 ± 1.04	[21]
19.5	11.9 ± 0.3	34.18 ± 7.00	162.01 ± 10.20	3.81 ± 1.36	this work
20	13.4	37.12 ± 5.01	158.35 ± 6.84	5.15 ± 2.47	[21]
29.1	13.7 ± 0.3	27.15 ± 5.17	165.29 ± 7.64	7.56 ± 1.97	this work
48.3	14.4 ± 0.3	24.95 ± 5.21	166.21 ± 9.76	8.83 ± 3.22	this work
30	14.7	28.83 ± 4.34	159.85 ± 8.36	10.90 ± 6.46	[21]
67.7	15.6 ± 0.3	22.44 ± 5.65	168.03 ± 8.88	9.53 ± 3.95	this work
70	19.9	22.84 ± 2.32	164.46 ± 4.24	13.33 ± 2.75	[21]
3500	50	16.1 ± 10.8	129.7 ± 19.3	54.1 ± 27.8	[17, 20]

weights obtained in this way were nearly identical to the results of Eq. (11), albeit with larger uncertainties.

Figure 4 shows the results of least-squares approximation of the obtained mass distributions using expression (11).

An important question which is connected to the discussion of fission modes is the dependence of the modes on the average excitation energy. Ref. [56] presented experimental yields of fragments with mass numbers $A = 134, 139, 143$ as a function of the excitation energy in photofission of ^{238}U. The $A = 134$ yield decreases from 9% to 6% as the excitation energy increases from 6 to 20 MeV, while the yields of fragments with $A = 139, 143$ practically do not change within error boundaries. Although this behavior gives general description of the energy dependence of the contribution of asymmetric modes STI and STII, it does not provide quantitative estimates of probabilities of the modes. Furthermore, it is shown in the works that analyzed the photofission modes of ^{238}U [19] and neutron-induced fission of ^{235}U [15, 57], that the width of the STI mode is approximately two times less than the width of STII, and, hence, it not enough to compare just the yields of specific mass chains, i.e. the amplitudes of the modes, but one has to take into account the areas of the corresponding distributions. Only one work, namely Ref. [17], contains calculation of contributions of fission modes into the mass distribution, while in other works on photofission such analysis has not been made. [18] merely points at the presence of three distinct fission modes in the experimental data. In [19] the contributions of the fission modes are estimated from the mass-energy spectra of the fragments of fission induced by bremsstrahlung radiation at electron accelerator energies from 6 to 10 MeV.

To analyze the contribution of photofission modes of ^{238}U we used our data and the data from Refs. [17, 18, 20–22], where the authors provided an estimation of the average excitation energy. In these works the mass distributions were obtained after the emission of prompt neutrons, i.e. the post-neutron distributions were measured. The experimental mass distributions from Refs. [17, 18, 20–22] were also decomposed into Gaussian functions, and, according to Eq. (11), the contributions, or weights, of each mode were obtained in each case as $W = K\sqrt{2\pi\sigma^2}$, where K and σ correspond to the parameters of the mode.

Presence of three fission modes has been found in all of the measured and analyzed mass distributions at excitation energies $\langle E^* \rangle > 10$ MeV. Table II lists the obtained contributions of the fission modes of ^{238}U to the resulting mass distribution at different mean excitation energies $\langle E^* \rangle$. At lower excitation energies the weight of the symmetric SL mode is expected to be less than 1% and no decays with mass numbers $110 < A < 127$ were detected in [18] in post-neutron distributions using the activation technique. At the same time in both works [18, 19] using the double energy technique a small contribution of the symmetric fission is observed in the pre-neutron distributions. The analysis of the obtained data shows that the contribution of the symmetric fission mode increases by about an order of magnitude as the excitation energy increases from 9 to 20 MeV. The contribution of the asymmetric mode STI, related to the spherical neutron shell $N = 82$ drops in about two times in the same energy range. The contribution of the asymmetric mode STII, related to the deformed neutron shell $N = 86 \div 88$ increases.

It has been shown previously from the analysis of the peak-to-valley ratios, that the ratio of asymmetric and symmetric fission decreases exponentially as the excitation energy increases. However, this dependence as is is probably not a direct reflection of the behavior of shell effects in this range of the excitation energy of the

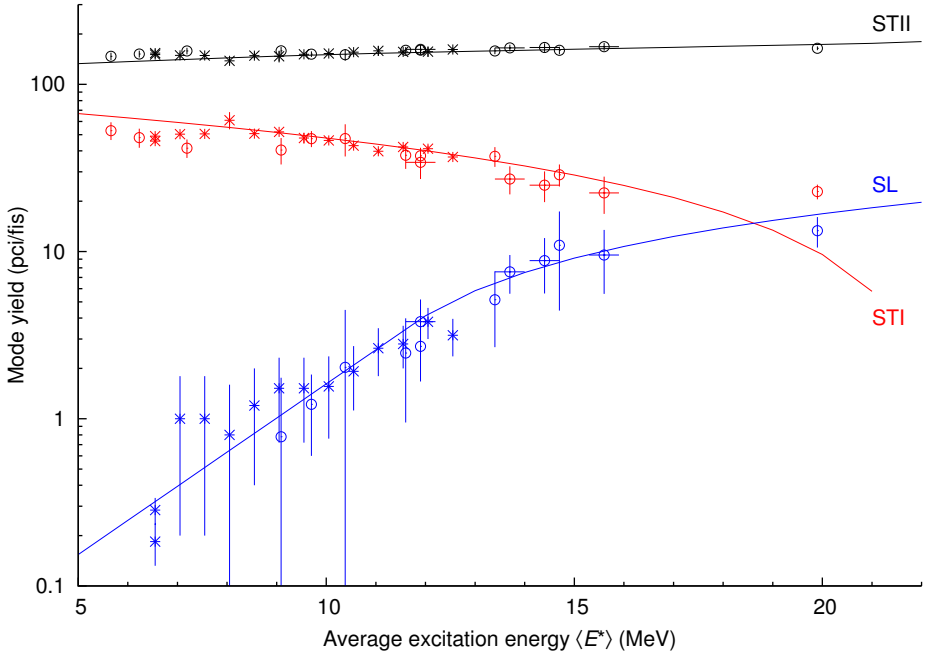

Figure 7. (Color online) Contributions (weights) of different fission modes in photofission of ^{238}U and neutron-induced fission of ^{235}U as a function of the average excitation energy $\langle E^* \rangle$: (circles) contributions of the STII, STI, SL modes of photofission of ^{238}U calculated from mass distributions obtained in the present work and in works [17, 18, 20–22], (stars) contributions of the STII, STI, SL modes of neutron-induced fission of ^{235}U from [15]. Mode yields are normalized per 100 fission reactions: $Y_{SL} + Y_{STI} + Y_{STII} = 200\%$.

fissioning nucleus. This can be seen from the behavior of the two asymmetric modes which both appear due to the shell correction component of the fission barrier, and only one of these modes drops with the increase of the excitation energy.

It has been shown above that the ratio between asymmetric and symmetric fission for photofission of ^{238}U and fission of ^{235,238}U induced by monoenergetic neutrons are very close. In the following comparison of the relative contributions of modes in photon- and neutron-induced fission we used the data from [15], where the relative contributions of the modes were obtained up to the excitation energy of 12 MeV. For comparison of the fission modes in the whole studied energy range we used the fission product systematics in proton- and neutron-induced fission from [16]. Figure 7 shows the relative contributions of fission modes during photofission of ^{238}U and neutron-induced fission of ^{235}U [15]. Curves denote results of calculation of fission of a compound nucleus of uranium with $A = 238$, according to the systematics from [16]. It is seen that the energy dependence of modes in photofission of ^{238}U and neutron-induced fission of ^{235}U is identical, which is a common but not general behavior: e.g., there is a very pronounced difference in energy dependencies of peak-to-valley ratios of thorium isotopes [56].

The behavior of the STI mode, which is related to the $N = 82$ shell and the structure of the mass distribution around $A = 134$ agrees with the experimental data up to the excitation energy 15 MeV. However, one has to bear in mind that the systematics of Ref. [16] is composed in such a way that the STI contribution is zero at the energy $E = 22$ MeV, and there is only one experimental value of the contribution of modes in photofission of ^{238}U around 20 MeV.

At higher excitation energies (the last row of table II) there is a noticeable difference between the contributions of fission modes in photon- and neutron-induced fission. It follows from the systematics [16] that above 25 MeV there is no contribution of the STI mode. However, it is seen from the experimental results of [17, 20] that this mode is still present at 50 MeV. This behavior is further confirmed by measurements of the ratio of the asymmetric and symmetric channels [58]. Theoretical calculations of photofission probabilities at intermediate energies [59] suggest a rather different process of formation of final mass distributions due to hadron photoproduction cascades at the initial stage of photoabsorption.

IV. CONCLUSIONS

Photon activation technique was used to obtain photofission mass distributions of ^{238}U in a bremsstrahlung beam with end-point energies 19.5, 29.1, 48.3, and 67.7 MeV. The weights of the symmetric (SL) and asymmetric

(STI and STII) modes in the mass distributions of photofission of ^{238}U at the average excitation energies of up to 20 MeV are calculated on the basis of the obtained results and other available data.

Since the yield of each fission mode is determined by the probability of tunneling through a fission barrier, the observed distinctive behavior of the fission modes is an evidence of presence of three minimal trajectories, or three distinct fission barriers on the potential energy surface.

Damping of the shell effects results in an increase of the contribution of the symmetric mode SL, which increases by about an order of magnitude as the excitation energy increases from 9 to 20 MeV.

The weights of the asymmetric modes STI and STII and their energy dependence are noticeably different. This difference also implies substantially different shapes of the barriers for these fission modes.

The behavior of the asymmetric modes is anti-correlated. The contribution of the STI mode decreases by about 2.5 times from 5 to 20 MeV, the contribution of the STII mode slightly increases. This may be interpreted as an indication that the minima of the potential energy surface that correspond to asymmetric fission split before the saddle point, directly after the second potential well. The opposite behavior of the asymmetric modes can indicate not only different values of the shell corrections, but also of different dependencies of the shell corrections on the excitation energy, i.e. different shell effects damping functions.

[1] C. D. Bowman *et al.*, Nucl. Instrum. Methods A **320**, 336 (1992).
[2] S. Leray *et al.*, Phys. Rev. C **65**, 044621 (2002).
[3] K. W. D. Ledingham and W. Galster, New J. Phys. **12**, 045005 (2010).
[4] D. J. S. Findlay, Nucl. Instrum. Methods B **50**, 314 (1990).
[5] D. Ene, C. Borcea, S. Kopecky, W. Mondelaers, A. Negret, and A. J. M. Plompen, Nucl. Instrum. Methods A **618**, 54 (2010).
[6] S. S. Belyshev, A. N. Ermakov, A. A. Kuznetsov, I. V. Makarenko, and V. V. Khankin, Moscow Univ. Phys. Bull. **62**, 360 (2007).
[7] A. J. Koning, S. Hilaire, and M. C. Duijvestijn, in *Proceedings of the International Conference on Nuclear data for Science and Technology, Nice, France, 2007*, edited by O. Bersillon, F. Gunsing, E. Bauge, R. Jacqmin, and S.Leray, (EDP Sciences, 2008), p. 211.
[8] M. Herman, R. Capote, B. V. Carlson, P. Obložinský, M. Sin, A. Trkov, H. Wienke, and V. Zerkin, Nucl. Data Sheets **108**, 2655 (2007).
[9] U. Brosa, S. Grossmann, and A. Müller, Phys. Rep. **197**, 167 (1990).
[10] P. Möller, A. J. Sierk, T. Ichikawa, A. Iwamoto, R. Bengtsson, H. Uhrenholt, and S. Åberg, Phys. Rev. C **79**, 064304 (2009).
[11] V. M. Strutinsky, Nucl. Phys. A **95**, 420 (1967).
[12] M. C. Duijvestijn, A. J. Koning, and F.-J. Hambsch, Phys. Rev. C **64**, 014607 (2001).
[13] A. V. Ignatyuk, K. K. Istekov, and G. N. Smirenkin, Sov. J. Nucl. Phys. **29**, 450 (1979).
[14] P. Möller and J. Randrup, Phys. Rev. C **88**, 064606 (2013).
[15] U. Brosa, H.-H. Knitter, T.-S. Fan, J.-M. Hu, and S.-L. Bao, Phys. Rev. C **59**, 767 (1999).
[16] A. C. Wahl, Los Alamos Report No. LA-13928, 2002.
[17] N. A. Demekhina and G. S. Karapetyan, Phys. At. Nucl. **71**, 27 (2008).
[18] S. Pommé, E. Jacobs, M. Piessens, D. De Frenne, K. Persyn, K. Govaert, and M. -L. Yoneama, Nucl. Phys. A **572**, 237 (1994).
[19] A. Göök, M. Chernykh, C. Eckardt, J. Enders, P. von Neumann-Cosel, A. Oberstedt, S. Oberstedt, and A. Richter, Nucl. Phys. A **851**, 1 (2011).
[20] A. Deppman, E. Andrade-II, V. Guimarães, G. S. Karapetyan, and N. A. Demekhina, Phys. Rev. C **87**, 054604 (2013).
[21] E. Jacobs, H. Thierens, D. De Frenne, A. De Clercq, P. D'hondt, P. De Gelder, and A. J. Deruytter, Phys. Rev. C. **21**, 237 (1980).
[22] H. Naik, F. Carrel, G. N. Kim, F. Laine, A. Sari, S. Normand, and A. Goswami, Eur. Phys. J. A **49**, 94 (2013).
[23] B. S. Ishkhanov and A. A. Kuznetsov, Moscow Univ. Phys. Bull. **68**, 279 (2013).
[24] S. S. Belyshev, A. N. Ermakov, B. S. Ishkhanov, V. V. Khankin, A. S. Kurilik, A. A. Kuznetsov, V. I. Shvedunov, and K. A. Stopani, Nucl. Instrum. Methods A **745**, 133 (2014).
[25] S. S. Belyshev and K. A. Stopani, Moscow Univ. Phys. Bull. **68**, 88 (2013).
[26] B. S. Ishkhanov and A. A. Kuznetsov, Phys. At. Nucl. **77**, 824 (2014).
[27] V. I. Shvedunov *et al.*, Nucl. Instrum. Methods A **550**, 39 (2005).
[28] A. C. Wahl, R. L. Ferguson, D. R. Nethaway, D. E. Troutner, and K. Wolfsberg, Phys. Rev. **126**, 1112 (1988).
[29] A. C. Wahl, At. Data Nucl. Data Tables **39**, 1 (1988).
[30] N. Sugarman and A. Turkevich, in *Radiochemical Studies: The Fission Product*, edited by C. D. Coryell and N. Sugarman, Vol. 3 (Mc Graw-Hill, New York, 1951), p. 1396
[31] H. N. Erten and N. K. Aras, J. Inorg. Nucl. Chem. **41**, 149 (1979).
[32] D. De Frenne, H. Thierens, B. Proot, E. Jacobs, P. De Gelder, A. De Clercq, and W. Westmeier, Phys. Rev. C **26**, 1356 (1982).
[33] S. Pommé, E. Jacobs, K. Persyn, D. De Frenne, K. Govaert, and M.-L. Yoneama, Nucl. Phys. A **560**, 689 (1993).
[34] D. De Frenne, H. Thierens, B. Proot, E. Jacobs, P. De Gelder, and A. De Clercq, Phys. Rev. C **29**, 1908 (1984).

[35] S. Agostinelli *et al.*, Nucl. Instrum. Methods Phys. A **506**, 250 (2003).
[36] J. T. Caldwell, E. J. Dowdy, B. L. Berman, R. A. Alvarez, and P. Meyer, Phys. Rev. C **21**, 1215 (1980).
[37] A. Veyssière, H. Beil, R. Bergère, P. Carlos, J. Fagot, A. Leprêtre, and J. Ahrens, Nucl. Instrum. Methods **165**, 417 (1979).
[38] J. D. T. Arruda Neto, S. B. Herdade, B. S. Bhandari, and I. C. Nascimento, Phys. Rev. C **14**, 1499 (1976).
[39] V. V. Varlamov and N. N. Peskov, Moscow State Univ. Inst. of Nucl. Phys. Reports, No. 2007, 829 (2007)
[40] B. S. Ishkhanov and A. A. Kuznetsov, Moscow. Univ. Phys. Bull. **68**, 27 (2013).
[41] A. Turkevich and J. B. Niday, Phys. Rev. **84**, 52 (1951).
[42] R. A. Schmitt and N. Sugarman, Phys. Rev. **95**, 1260 (1954).
[43] E. Jacobs, H. Thierens, D. De Frenne, A. De Clercq, P. D'hondt, P. De Gelder, and A. J. Deruytter, Phys. Rev. C **19**, 422 (1979).
[44] H. Thierens, D. De Frenne, E. Jacobs, A. De Clercq, P. D'hondt, and A. J. Deruytter, Phys. Rev. C **14**, 1058 (1976).
[45] A. Chattopadhyay, K. A. Dost, I. Krajbich, and H.D. Sharma, J. Inorg. Nucl. Chem. **35**, 2621 (1973).
[46] H. Naik *et al.*, Nucl. Phys. A **853**, 1 (2011).
[47] L. E. Glendenin, J. E. Gindler, D. J. Henderson, and J. W. Meadows, Phys. Rev. C **24**, 2600 (1981).
[48] T. R. England and B. F. Rider, Los Alamos National Laboratory Reports LA-UR-94-3106, ENDF-349, 1993 (unpublished).
[49] D. E. Adams, W. D. James, J. N. Beck, and P. K. Kuroda, J. Inorg. Nucl. Chem. **37**, 419 (1975).
[50] S. Nagy, K. F. Flynn, J. E. Gindler, J. W. Meadows, and L. E. Glendenin, Phys. Rev. C **17**, 163 (1978).
[51] N. L. Borisova, S. M. Dubrovina, V. I. Novgorodtseva, V. A. Pchelin, V. A. Shigin, and V. M. Shubko, Sov. J. Nucl. Phys. **6**,331 (1968).
[52] J. T. Harvey, D. E. Adams, W. D. James, J. N. Beck, J. L. Meason, and P. K. Kuroda, J. Inorg. Nucl. Chem. **37**, 2243 (1975).
[53] T. C. Chapman, G. A. Anzelon, G. C. Spitale, and D. R. Nethaway, Phys. Rev. C **17**, 1089 (1978).
[54] M. Rajagopalan, H. S. Pruys, A. Grütter, E. A. Hermes, and H. R. von Gunten, J. Inorg. Nucl. Chem. **38**, 351 (1976).
[55] W. Gunther, K. Huber, U. Kneissl, H. Krieger and H. J. Maier, Z. Physik A **295**, 333 (1980).
[56] H. Naik, A. Goswami, G. N. Kim, M. W. Lee, K. S. Kim, S. V. Suryanarayana, E. A. Kim, S. G. Shin, and M.-H. Cho, Phys. Rev. C **86**, 054607 (2012).
[57] N. Zheng, T.-S. Fan, Y. Ding, C.-L. Zhong, X.-Q. Li, and J.-X. Chen, Chin. Phys. C **34**, 49 (2010).
[58] D. I. Ivanov, G. Ya. Kezerashvili, V. G. Nedorezov, A. S. Sudov, and A. A. Turinge, Sov. J. Nucl. Phys. **55**, 1464 (1992).
[59] I. A. Pshenichnov, B. L. Berman, W. J. Briscoe, C. Cetina, G. Feldman, P. Heimberg, A. S. Iljinov, and I. I. Strakovsky, Eur. Phys. J. A **24**, 69 (2005).